Many-body Correlations and Exciton Complexes in CsPbBr3 Quantum Dots

Chenglian Zhu, Tan Nguyen, Simon C Boehme, Anastasiia Moskalenko, Dmitry N Dirin, Maryna I Bodnarchuk, Claudine Katan, Jacky Even, Gabriele Rainò, Maksym V Kovalenko

ADVANCED MATERIALS
www.advmat.de

Many-Body Correlations and Exciton Complexes in $CsPbBr_3$ Quantum Dots

Chenglian Zhu, Tan Nguyen, Simon C. Boehme, Anastasiia Moskalenko, Dmitry N. Dirin, Maryna I. Bodnarchuk, Claudine Katan, Jacky Even, Gabriele Rainò,* and Maksym V. Kovalenko**

All-inorganic lead-halide perovskite (LHP) ($CsPbX_3$, X = Cl, Br, I) quantum dots (QDs) have emerged as a competitive platform for classical light-emitting devices (in the weak light–matter interaction regime, e.g., LEDs and laser), as well as for devices exploiting strong light–matter interaction at room temperature. Many-body interactions and quantum correlations among photogenerated exciton complexes play an essential role, for example, by determining the laser threshold, the overall brightness of LEDs, and the single-photon purity in quantum light sources. Here, by combining cryogenic single-QD photoluminescence spectroscopy with configuration-interaction (CI) calculations, the size-dependent trion and biexciton binding energies are addressed. Trion binding energies increase from 7 to 17 meV for QD sizes decreasing from 30 to 9 nm, while the biexciton binding energies increase from 15 to 30 meV, respectively. CI calculations quantitatively corroborate the experimental results and suggest that the effective dielectric constant for biexcitons slightly deviates from the one of the single excitons, potentially as a result of coupling to the lattice in the multiexciton regime. The findings here provide a deep insight into the multiexciton properties in all-inorganic LHP QDs, essential for classical and quantum optoelectronic devices.

1. Introduction

Fully inorganic LHP ($CsPbX_3$, X = Cl, Br, I) QDs, first colloidally synthesized in 2015,[1] have been the focus of intense research efforts since then. Synthetic endeavor, which culminated in the presently available precise control over QD size, shape, and composition,[2,3] (see Figure S1, Supporting Information, for the TEM images) have largely been motivated by the near-unity photoluminescence quantum yield (PLQY), stemming from a defect tolerant electronic structure, and a narrow PL band, tunable across the entire visible spectral region.[1,2,4–6] These compelling material properties have already enabled superior performance of optoelectronic devices exploiting $CsPbX_3$ QDs, for example, LEDs with external quantum efficiencies above 20%,[7–10] lasers with wide spectral tunability,[11–16] and photodetectors with record-high responsivity.[17–20] In addition to the development of classical light emitting devices, $CsPbX_3$ QDs are also conceived as sources of quantum light, being capable of either delivering single photons[21–29] or bunched (temporally correlated) N-photon bundles,[30] enabled by a fast radiative decay (sub-ns)[28,29,31] and a long exciton coherence.[29,32,33] Similarly, exploiting the strong light–matter interaction regime represents the tantalizing perspective of realizing room-temperature (RT) exciton–polaritonics operating at the quantum level.[34] For the latter, it is crucial to optimally utilize the sizable many-body interactions in perovskite QDs, with the ultimate goal of demonstrating a strong nonlinearity down to the single-photon level, as has been recently reported

C. Zhu, S. C. Boehme, A. Moskalenko, D. N. Dirin, G. Rainò, M. V. Kovalenko
Institute of Inorganic Chemistry
Department of Chemistry and Applied Biosciences
ETH Zürich
Zurich CH-8093, Switzerland
E-mail: rainog@ethz.ch; mvkovalenko@ethz.ch

The ORCID identification number(s) for the author(s) of this article can be found under https://doi.org/10.1002/adma.202208354.

DOI: 10.1002/adma.202208354

C. Zhu, S. C. Boehme, A. Moskalenko, D. N. Dirin, M. I. Bodnarchuk, G. Rainò, M. V. Kovalenko
Laboratory for Thin Films and Photovoltaics
Empa - Swiss Federal Laboratories for Materials Science and Technology
Dubendorf CH-8600, Switzerland

T. Nguyen, C. Katan
Univ Rennes
ENSCR
CNRS
ISCR – UMR6226
Rennes F-35000, France

J. Even
Univ Rennes
INSA Rennes
CNRS
Institut FOTON – UMR6082
Rennes F-35000, France
E-mail: jacky.even@insa-rennes.fr

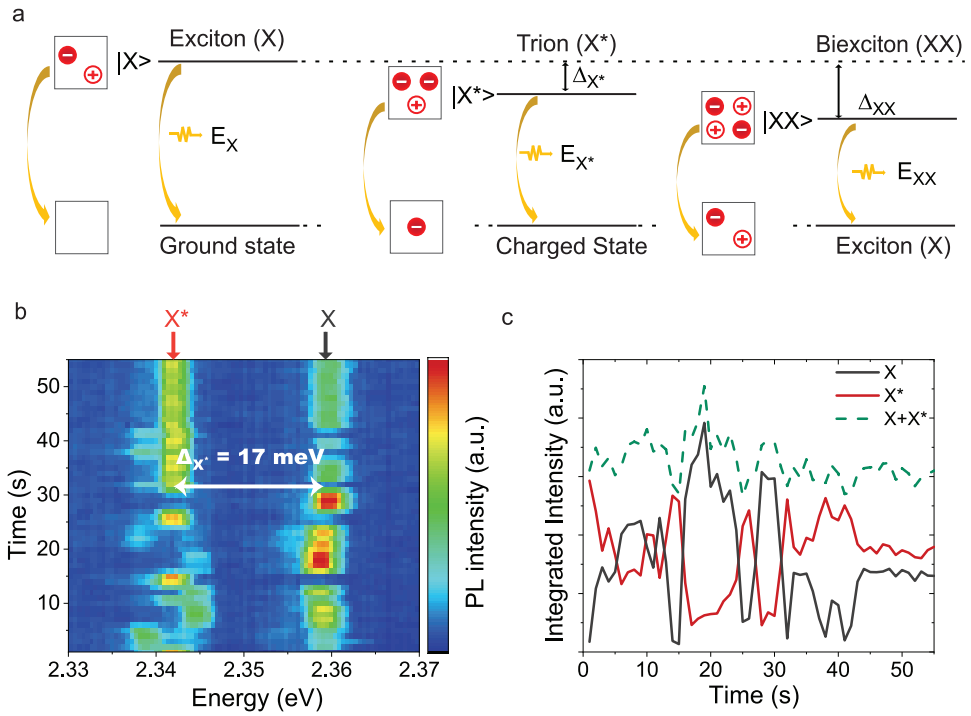

Figure 1. Fundamental properties of many-body interactions in a single $CsPbBr_3$ QD. a) Radiative recombination scheme of an exciton, trion (here depicted for the case of a negatively charged exciton), and biexciton, respectively. The emitted photon has an energy of E_X, E_{X^*} and E_{XX}, respectively. b) Time series of PL spectra from a single ≈9 nm $CsPbBr_3$ QD at 4 K, acquired with 1 s binning time. The two peaks are attributed to the exciton and a red-shifted trion recombination, respectively. c) Intensity time-trace of the exciton and trion from (b). The integrated intensity of each species is inferred from a double-Lorentzian fitting of the acquired spectra.

for a polymer embedded in a dielectric microcavity.[35] We anticipate that such a demonstration is also within reach for perovskite QD exciton polaritons, once the current knowledge gap on many-body excitonic interactions in perovskite QDs is addressed. In the following, we will delineate how our study attempts to provide a comprehensive description of many-body excitonic interactions in perovskite QDs.

The many-body interaction in exciton complexes can be probed by studying the binding energies of bound multiexciton species. In the simplest case, after optical excitation, a single exciton is created, that is, an electron in the conduction band Coulombically bound to a hole in the valence band. The radiative decay of such an exciton generates a photon at energy E_X (see left sketch in **Figure 1**a). Multiexciton complexes, that is, trions and biexcitons, can be created at high excitation densities. The trion, also known as charged exciton, is a three-charges complex, which can be formed when an exciton is created in the presence of an unpaired charge carrier in the QD. A negatively (positively) charged exciton is comprised of two electrons (holes), which share the same energy level, and one hole (electron), bound through the Coulomb interaction. Photons emitted from the trion configuration have energy E_{X^*} (see the middle sketch in Figure 1a exemplifying a negative trion).

A biexciton refers to two bound electron–hole pairs, which can be formed when exciton is created in the presence of another exciton already in the QD. The biexciton decays via a cascade process, sequentially transitioning from the biexciton state to the exciton state and, finally, to the ground state. Photons emitted from the biexciton configuration in transitioning to single exciton state possess an energy E_{XX} (see right sketch in Figure 1a).

Generally, E_{X^*} (E_{XX}) differs from E_X due to the many-body Coulombic interaction among the photogenerated charges. Consequently, the energy shift of the PL of a trion (biexciton) with respect to the exciton can serve as a probe of the correlation effects within a single QD, and the trion (biexciton) binding energy is usually defined as $\Delta_{X^*} = E_X - E_{X^*}$ ($\Delta_{XX} = E_X - E_{XX}$). In most studied colloidal QDs, trion emission is altered by non-radiative Auger recombination which dominates at RT, correlated with PL intensity intermittency.[23,36] Conversely, at cryogenic temperatures, the trion has been reported as a bright and narrow PL peak in LHP QDs[26,28,31,37–43] and other semiconductor QDs/QWs[44–53] with typically positive trion binding energies, that is, red-shifted trion emission. In extreme situations with strong internal piezoelectric field and large mass mismatch between the electrons and the holes, opposite binding behavior between positively and negatively charged trions in buried III-V QDs has been reported.[54] In contrast, the biexciton binding energy depends on a fine balance between attractive and repulsive interaction, while usually dominated by attractive interaction in type-I QDs due to the correlation energy of the confined excitons overwhelming the Coulombic repulsion.[55–57] In the case of a strong internal electric field, it has been shown that including correlation effects in the simulation of the biexciton ground state is necessary to reproduce the cross-over from binding to anti-binding as a function of the size in III-V QDs.[54] The biexciton binding energies in perovskite semiconductors have been intensively characterized via a

broad range of methods, for example, heralded spectroscopy,[55] transient absorption,[58–61] time-resolved PL trace,[62,63] and 2D electronic spectroscopy.[64] Note that care needs to be exercised when comparing results from either single or ensemble measurements, acquired at either RT or cryogenic temperature. For example, the reported values for Δ_{XX} in $CsPbBr_3$ QDs span the large range of –100 to +100 meV,[13,55,59,60,62,63,65–67] largely contradicting each other. We posit that single-QD PL spectroscopy at low temperatures is a promising route to lower the current uncertainty on many-body interactions, as this method allows for direct observation of individual multiexciton bands which typically feature significant spectral overlap at RT. However, biexciton emission studies via cryogenic single-QD PL spectroscopy have so far only been reported for $CsPbI_3$ QDs, with a very limited QD size range.[38,41] The current lack of further reports, also on other $CsPbX_3$ QD systems, stems from the typically sub-optimal optical and/or structural stability of perovskite QDs at high excitation densities and the typically efficient nonradiative Auger recombination of multiexcitons.[68,69] Despite the clear importance of multiexcitons, exciton–exciton interaction as well as multiexciton–phonon coupling are still poorly understood, both experimentally and theoretically.

In this work, we report on the size dependence of trion and biexciton binding energies of single $CsPbBr_3$ QDs across a broad size range to unveil the many-body interactions in such unusually soft inorganic semiconductors. We combined single-QD PL spectroscopy at cryogenic temperatures with theoretical calculations based on a configuration interaction (CI) method to gauge the importance of many-body effects. In the following, we will first discuss the spectral dynamics of trions and then assess their size-dependent binding energies (Δ_{X^*}). Next, we will show optical properties of biexcitons, that is, fine structure, fluence dependence, and size-dependent binding energies (Δ_{XX}). At the same time, CI calculations under effective mass approximation (EMA) on $CsPbBr_3$ QDs are presented and return specifics of soft perovskite compounds, for example, polaronic coupling in the multiexciton regime.

2. Results

2.1. Size-Dependent Trion Binding Energy

The $CsPbBr_3$ QDs used in this study were synthesized according to refs. [4] and [70]. The studied QDs have average edge lengths of ≈9, 13, 16, 23, and 30 nm. The ensemble absorption and PL spectra as well as TEM images and size distributions are presented in Figure S1, Supporting Information.

Figure 1b displays the time series of PL spectra of a single 9 nm $CsPbBr_3$ QD, obtained at cryogenic temperature. Two spectral emission lines are discernible, subject to both spectral diffusion as well as discrete exchanges of intensity between both lines. The latter would not be observed for phonon replica and biexcitons, since fluctuations in intensity and/or spectral position of the exciton typically occur in concert with either biexciton[38,41] or phonon replica.[41] In contrast, intensity fluctuations between both bands are well explained by photocharging events which transfer the photoexcited QD from the exciton state (neutral, with PL at higher energy) to the trion state (charged, with PL at lower energy), and vice versa in discharging events. In line with previous reports,[31,37–42] the photo-charging and -discharging processes seem to occur in a random fashion, and the residence times in the trion state depend on the excitation fluence, vary from QD to QD, and are sensitive to the dynamics of the surface/environment. For some QDs, multiple trion emission levels can be discerned (see Figure 1b), originating mainly due to fast spectral diffusion. By performing a double-Lorentzian fitting of each spectrum in the time series (details see Supporting Information), we extract the dynamics of PL energy, linewidth, and intensity of each band. Both exciton and trion band feature a linewidth of ≈1–2 meV, close to the spectral resolution of our monochromator (≈1 meV with a grating of 300 lines/mm). Under this experimental condition, we do not resolve the exciton fine-structure. Their intensities as a function of time are shown in Figure 1c, suggesting that the integrated intensities of the exciton and trion PL are very similar and their sum is constant, that is, exciton and trion exhibit comparable PLQY.[28] For the trion binding energy, we obtain $\Delta_{X^*} \approx 17$ meV for this 9-nm $CsPbBr_3$ QD, well within the broad range of 6–24 meV reported for 8–10 nm QDs in ref. [37].

By performing such measurements and analysis on QDs covering a broad range of sizes (see Figure S1, Supporting Information), we are able to quantify the dependence of Δ_{X^*} on QD size (or exciton energy). The representative time series of PL spectra from a 9-nm and a 30-nm QD are shown in **Figures 2**a,b, respectively, with clear spectral and intensity jump as well as bright emission of both exciton and trion. For the larger QD, we observe a clear decrease of Δ_{X^*} from 21 meV down to 8 meV together with a red-shift of the exciton from 2.374 to 2.338 eV due to the weaker quantum confinement. In total, we extracted Δ_{X^*} for over 100 single $CsPbBr_3$ QDs (under 0.11–7.5 μJ cm^{-2}) by measuring from the intermediate to weak quantum confinement regime. Figure 2c shows the trion binding energies (Δ_{X^*}) as a function of exciton energies (E_X) for all individual QDs as well as the mean value for each QD batch. QDs displayed in Figures 2a and 2b are marked by hollow dots, respectively, in Figure 2c. With decreasing QD size (mean exciton energy increasing from 2.32 to 2.42 eV), the mean trion binding energy increases from 7 ± 1 to 17 ± 3 meV. Since smaller QDs (9–13 nm) are more vulnerable to the surface/environment fluctuations, their spectra display stronger spectral diffusion (see Figures 1b and 2a) and therefore larger error bars in Δ_{X^*} (see Figure 2c,d). Figure 2d reports the mean values of Δ_{X^*} (blue solid) as a function of QD size, which agree well to previously reported results (Fu et al.[37] and Becker et al.[42]). The observed increase in trion binding energy for decreasing QD size is consistent with the enhanced Coulomb interaction between electrons and holes in stronger quantum confinement.

In the following, we will address the questions of 1) why trion binding energies in $CsPbBr_3$ QDs are high compared to epitaxial, for example, GaAs and InAs QDs/QWs,[51–53] and 2) which factors contribute to the size dependence of the trion binding energy in $CsPbBr_3$ QDs. To unveil the origin behind the large Δ_{X^*} in $CsPbBr_3$ QDs, especially at small QD size, we perform theoretical calculations considering parameters relevant to the orthorhombic crystal phase at low temperature, with a reduced effective mass $\mu = 0.126$, and an effective dielectric

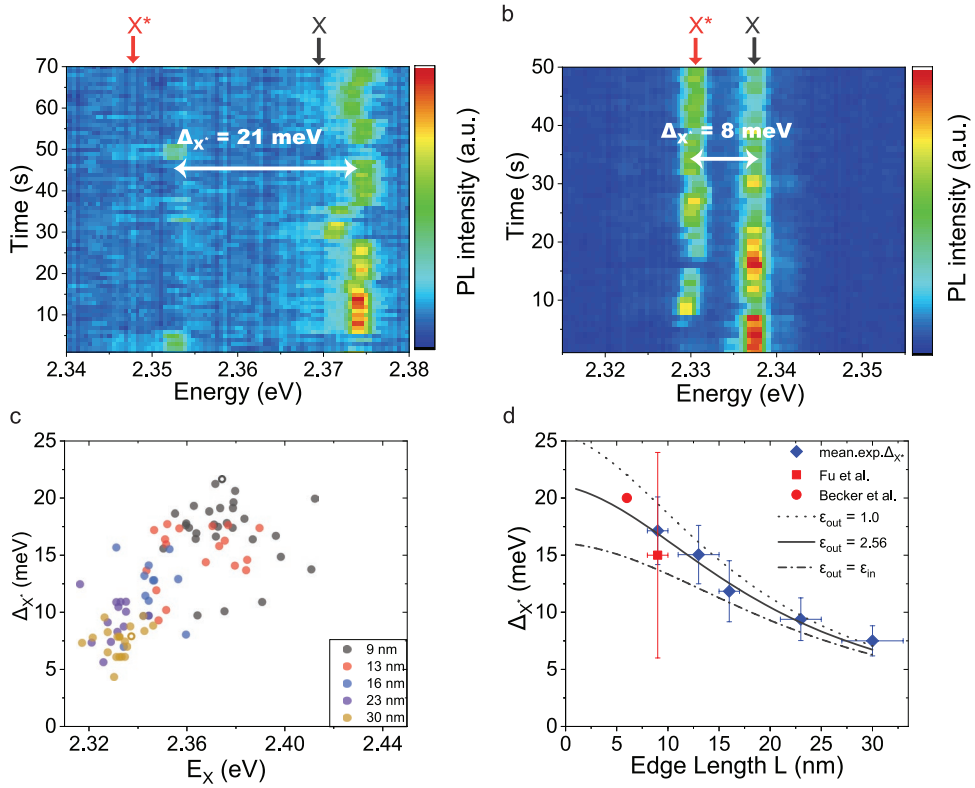

Figure 2. Size-dependent trion binding energy in $CsPbBr_3$ QDs. a,b) Time series of PL spectra from a single $CsPbBr_3$ QD with an edge length of ≈9 nm (a) and ≈30 nm (b), acquired with 1 s binning time. The trion binding energy (Δ_{X^*}), indicated by white arrows, is reduced in the larger QD. c) Experimental Δ_{X^*} of single QDs from QD batches with different mean QD sizes (see the legend for the color coding), reported as a function of the exciton energies (1s–1s transition). The single QDs depicted in (a) and (b) are displayed as the hollow dots. d) Trion binding energy as a function of size. Our experimental data (blue diamonds) are averaged over all the single QDs within one batch. Error bars are the standard deviation of Δ_{X^*} within each sample. CI calculations are performed without reduced dielectric constant in the environment (dash–dot line), for the experimentally employed polystyrene environment ($\varepsilon_{out} = 2.56$, solid line), and an air/vacuum environment ($\varepsilon_{out} = 1.0$, dot line). The best agreement with both our own experimental data as well as those reported by Fu et al.[37] with single QDs in PMMA (red cube) and Becker et al.[42] with single QDs in SEBS (red dot) is achieved by the CI calculation specifically accounting for the reduced dielectric screening by the employed polystyrene matrix. More details of CI calculations can be found in the Supporting Information.

constant $\varepsilon_{eff} = 7.3$ (see detailed discussion in Supporting Information).

First, we perform calculations using the well-established single-band EMA combined with a treatment of the quantum correlations between the carriers up to second order of many-body perturbation theory, as shown in Figure S3a, Supporting Information, where the predicted trion binding energies are systematically lower than the experimental data. As discussed in ref. [71], this underestimation could plausibly be explained by a combination of a slightly overestimated dielectric constant and/or so far neglected third- and higher-order terms in the correlation energy. To further refine the theoretical model, we performed additional calculations based on the full CI method under single-band EMA. Further details of the theoretical methods and assumptions can be found in Section SII, Supporting Information. Theoretical calculations considering different environment dielectric constant (ε_{out}) are plotted and compared in Figure 2d.

A first scenario $\varepsilon_{out} = \varepsilon_{eff} = 7.3$ (dash–dot grey line) mimics the case of a densely packed QD ensemble (e.g., in a thin film), where QDs are surrounded by other QDs with the same effective dielectric constant. Clearly, such a scenario still underestimates the experimental values. In the second scenario, we consider QDs in the vacuum with $\varepsilon_{out} = 1$, where results predict higher binding energy compared to experimental values. In the last scenario, we consider QDs embedded in a dielectric matrix with lower dielectric constant, which is the case of our single-QD experiment where we have embedded our single QDs in a polystyrene (PS) matrix to enhance the stability[2,72–77] (see the Experimental Section for details about the sample preparation). In this scenario, the theoretical calculations include the approximate effect of dielectric confinement as detailed in Section SII, Supporting Information. With the dielectric constant $\varepsilon_{out} = 2.56$ for PS, an excellent agreement with the experimentally derived values is reached. The developed theoretical model can further predict trion binding energies in QDs with different compositions, for example, weakly confined (≈30 nm) $CsPb(Br/Cl)_3$ QDs obtained by performing anion exchange on $CsPbBr_3$ samples of the same size. On average, we find higher trion binding energies after the anion exchange, as shown in Figure S4, Supporting Information. CI calculations for PS-encapsulated QDs again yield a good agreement with the experimental values. Hence, apart from the above established effect of size (via the quantum confinement), the perovskite

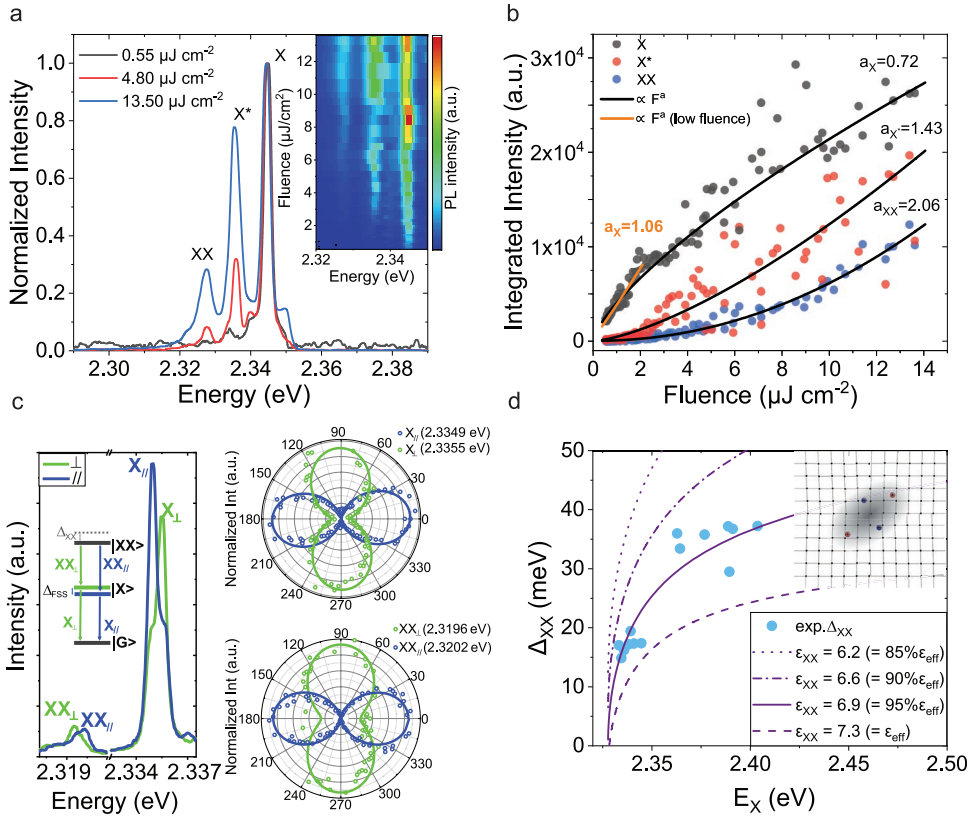

Figure 3. Size-dependent biexciton binding energy (Δ_{XX}) and polarization-dependent biexciton fine structure in single $CsPbBr_3$ QDs. a) PL spectra of a single ≈23 nm $CsPbBr_3$ QD at three different excitation fluences. Inset: Fluence-dependent PL spectra show the gradual emergence of the trion and biexciton peaks. The integration time of each spectrum is 1 s. b) Fluence dependence of the spectrally integrated intensity of the exciton peak (dark grey), trion peak (red), and biexciton peak (blue); power-law fits yield exponents of 0.72 (1.06 within low excitation regime), 1.43, and 2.06, respectively. c) Polarization-resolved exciton and biexciton fine structures from a single ≈30 nm QD. The left panel: PL spectra measured at the polarization angles of 0° (blue, labeled as//) and 90° (green, labeled as ⊥) for *X* and *XX* of a single $CsPbBr_3$ QD excited well above the saturation. Inset: schematic representing the polarization of photons generated via the cascade process from biexciton to exciton to ground state. The right two polar plots are PL intensities of the exciton (biexciton) doublet as a function of the linear polarizer angle. The blue (green) data points correspond to the exciton/biexciton doublet peak shown in the left panel with a low (high)/high (low) energy. d) Size-dependent biexciton binding energies from single QDs, expressed as a function of their single-exciton energies (1s–1s transition). A perfect match between experiment and theory in the case of $\varepsilon_{XX} = 6.9 = 95\%\varepsilon_{eff}$ suggest that the effective dielectric constant for QDs with a biexciton is reduced by 5% compared to a QD with a single exciton ($\varepsilon_X = \varepsilon_{eff} = 7.3$) with $\varepsilon_{out} = 2.56$ for PS. Inset: schematic representing the biexciton-induced lattice distortion. The latter results in an unconventionally high biexciton interaction, especially in strongly confined QDs.

composition is another tuning knob for controlling the trion binding energy, here achieved via a decrease of the dielectric constant to $\varepsilon_{eff} = 7.0$ after partial Br → Cl anion exchange in the mixed-halide $CsPb(Br/Cl)_3$ QDs.

2.2. Size-Dependent Biexciton Binding Energy

To identify the biexciton state, we study the PL spectra from single QDs under progressively high excitation fluences. **Figure 3**a shows the case of a 23 nm QD, which at low fluence (dark grey solid) predominantly exhibits PL from the exciton state (2.3445 eV), while at higher fluences (red and blue solid lines) two additional sharp peaks appear at lower energies (additional fluence-dependent measurements on different sized QDs are presented in Figures S6 and S7, Supporting Information). We attribute the latter to a trion and biexciton with an energy E_{X^*} (2.3358 eV) and E_{XX} (2.3280 eV), respectively. The inset shows the full fluence dependence with PL spectra acquired between 0.49 and 13.60 μJ cm^{-2}. With increasing fluence, first the trion and then the biexciton band significantly increase in relative strength. To further confirm the origin of the two red-shifted lines, we explore the fluence dependence of their respective intensities. After spectrally deconvoluting the respective lines via Lorentzian fits to the spectra, we plot, in Figure 3b, the integrated intensity of exciton (grey markers), trion (red markers), and biexciton (blue markers). Power-law fits (solid lines) to each of the three intensity traces (see Supporting Information for further details) reveal distinctly different behavior, with power-law exponents of 0.72 (1.06 within low excitation regime), 1.43 (up to high excitation regime), and 2.06 (up to high excitation regime) for exciton, trion, and biexciton, respectively. The super-linear fluence dependence of the trion and biexciton with exponents close to the expected values (≈1.5 and 2 for the trion and biexciton, respectively) corroborate our assignment of the emissive species.[26,38,78–80]

Having identified and assigned the biexciton band in the rich PL spectrum of colloidal $CsPbBr_3$ QDs, we now proceed to target an outstanding challenge in the colloidal QD field. Unlike for the well-studied and robust epitaxial QDs,[81–85] a thorough study of the biexciton fine structure with a full polarization dependence of each sub-level has still not been reported for $CsPbBr_3$ QDs, and only few reports exist employing $CsPbI_3$ QDs.[38,41] This can, in part, be attributed to the presently still limited photostability of perovskite QDs at the high excitation densities required for observing biexciton emission. Obtaining such knowledge would be important for unlocking the full potential of colloidal QDs for several quantum-technology applications.

Here, enabled by the latest development in the synthesis of bright and photostable QDs (see Supporting Information),[70] we report, to the best of our knowledge, for the first time the polarization dependence of the biexciton fine structure in $CsPbBr_3$ QDs. Consistently with previous reports,[31] trions emission has been found to be unpolarized (Figure S8, Supporting Information). In Figure 3c, the representative PL spectra excited at 1.50 μJ cm^{-2} (QD size ≈30 nm) at the polarizer angles of 0° (blue, labeled as//) and 90° (green, labeled as ⊥) are displayed. The spectra indicate spectral fingerprints of exciton and biexciton doublet fine-structure, with fine structure splitting (Δ_{FFS}) around 0.6 meV. In the right panel of Figure 3c, a polarization diagram is displayed for each studied structure, each point representing the integrated intensity of one peak at a given orientation. The linear and orthogonal polarization of this doublet is fully unveiled by these two polar plots. Comparing the two polar plots with the spectra, peak $X_{||}$ ($XX_{||}$) corresponds to the exciton (biexciton) doublet peak with the low (high) energy. The peak $X_{\perp}$ ($XX_{\perp}$) refers to the other sub-level. Single-exciton fine structures with linear and orthogonal polarization have been reported for perovskite QDs and associated to bright triplet exciton character.[28,31,37,38,86–88] For the biexciton, as the energy diagram depicted in the inset of Figure 3c, transition lines start from the bright biexciton state $|XX\rangle$ to the non-degenerate exciton triplet $|X\rangle$, and the latter to the ground state $|G\rangle$. Each pair of photons from $|XX\rangle$ to the ground state with $|X\rangle$ being an intermediate state should conserve the same total energy as well as polarization.[38,81–85] This is consistent with the symmetry analysis of the exciton and biexciton states in the orthorhombic phase of $CsPbBr_3$ (see Supporting Information). In conclusion, both the power-dependent measurements and the polarization resolved fine-structures in these large $CsPbBr_3$ QDs confirm our assignment to a biexciton, with an overall attractive exciton–exciton interaction. Weakly confined QDs (≈23–30 nm) exhibit biexciton binding energies Δ_{XX} of ≈15–18 meV. The biexciton binding energy can further be enhanced via the quantum confinement effect (by reducing the QD size), as shown in Figure 3d. When QD sizes decrease from 30 to 9 nm, the Δ_{XX} is doubled from ≈15 to 30 meV. For such small QDs, large spectral diffusion hinders the observation of biexciton fine structures. Remarkably, the biexciton binding energy is large and nearly equal to the exciton binding energy, contrary to standard semiconductors in which Δ_{XX} accounts for ≈20–30% of the exciton binding energy. This remarks the quite strong correlation of excitons in soft perovskite compounds.

As for the case of trions, Figure 3d compares the experimental data of biexciton binding energies with the theoretical predictions based on the developed CI model. CI calculations which include the sole, approximate environmental dielectric screening (purple dash) fail to reproduce the experimental trend, especially for small QD size. This is consistent with previous variational calculations on CdSe nanoplatelets, which demonstrate that the ratio of the biexciton to exciton binding energies remains smaller than the theoretical 2D limit of 0.23 when the same dielectric confinent effect is considered for both cases.[89,90] A so far missing contribution to the binding energy may come from the recently discussed photoinduced lattice deformations in metal-halide QDs and the formation of biexciton polarons,[58,67,91–95] a weak and generally neglected effect in conventional semiconductor QDs. It shall yield a polaronic interaction with the biexciton complex slightly different from the one of the excitons due to the non-negligible local lattice deformation and enhanced carrier correlations (see inset in Figure 3d). Specifically, we posit that the effect of polaron manifests itself as decreased dielectric constant in the biexciton regime (ε_{XX}). Tuning the ε_{XX} in the calculations, we found that a hypothetical 5% reduction in ε_{XX} compared to the effective dielectric constant of single exciton (ε_{eff}) well reproduces the experimental data. Such a limited, albeit important, lattice-mediated reduction in the dielectric constant for biexcitons may be one of the keys to rationalize the surprisingly high biexciton binding energy, and hence, strong multiexciton interaction in $CsPbX_3$ QDs, particularly in the strong confinement regime. In other words, our combined experimental–theoretical work suggests that colloidal perovskite QDs not only display remarkable optical properties in the single-exciton regime, but also unfold exciting and unconventional many-body interactions under strong optical excitations. From a theoretical perspective, it is important to note that the conjecture for lattice-mediated reduced dielectric constant of biexcitons can be rigorously assessed only when a full CI implementation, especially one that contains the triple and quadruple excitations, based on a more sophisticated model beyond EMA and an exact description of the dielectric screening are included.

3. Conclusion

In conclusion, we reveal the size-dependent trion and biexciton binding energy of $CsPbBr_3$ QDs via a combination of single-QD PL spectroscopy at cryogenic temperatures and calculations based on the CI method. Both the trion and biexciton interaction is attractive and the associated binding energies increase with decreasing QD size. The experimentally inferred size-dependent trion binding energies can be fully reproduced in our calculations after including the effects of quantum confinement, phonon screening due to exciton–phonon interaction, as well as dielectric screening by the environment. However, in the case of biexciton binding energies, satisfactory agreement between theory and experiment is only achieved after accounting for an altered effective dielectric medium. We posit that the latter is a result of photoinduced lattice distortions and biexciton–polaron formation in the soft host material, particularly important for smaller QDs. Our findings deepen

the understanding of many-body interactions in all-inorganic $CsPbX_3$ LHP QDs and serve as a basis for exploring the utilization of trions and biexcitons in quantum technologies, for example, single-photon sources, entangled-photon pair emission, and polaritonic devices.

4. Experimental Section

Sample Preparation: The preparation consisted of two major steps: dilution and spin coating. Both steps were conducted in a glove box under N_2 atmosphere. The QDs dispersion with a concentration of ≈0.5–1 mg mL^{-1} was diluted by a factor 100 to 200 in toluene (ACROS, 99.85% extra dry over molecular sieves). The solution was further diluted by another factor 100 in a 3-mass% solution of polystyrene (ALDRICH, average Mw ≈ 280 000) in toluene (ACROS, 99.85% extra dry over molecular sieves). 50 µL of the final solution was spin coated onto an intrinsic crystalline Si wafer with a 3-µm-thick thermal-oxide layer at 50 r.p.s for 60 s.

Optical Characterization: For single-QD spectroscopy, a home-built micro-PL setup was used. The samples were mounted on *xyz* nano-positioning stages inside an evacuated liquid-helium closed-loop cryostat (Montana Instruments) and cooled down to a targeted temperature of 4 K. Single QDs were excited by means of a fiber-coupled excitation laser at an energy of 3.06 eV with a repetition rate of 20 MHz (PicoQuant, <50 ps pulses) or at an energy of 2.58 eV with a repetition rate of 80 MHz (Toptica Photonics, 400 fs pulses), which was focused ($1/e^2$ radius = 1.2 µm) on the sample by a microscope objective (NA = 0.8, 100×). Typical power densities used to excite single QDs were 0.11–7.5 µJ cm^{-2}. The emitted light was collected by the same objective and passed through a dichroic mirror (long-pass, cut-on wavelength 450 nm or 488 nm) and a long-pass filter at 450 or 500 nm. The emitted light was analyzed by a monochromator coupled to an EMCCD (Princeton Instruments, 0.75 m, typical integration time of 1 s) for spectra measurements. Spectra could be measured with a grating of 300 lines/mm, blaze 500 nm, giving around 1 meV spectral resolution. Polarization resolved spectra were measured under 1.5 µJ cm^{-2} excitation, with a grating of 1800 lines/mm, blaze 500 nm (≈0.3 meV resolution), and a linear polarizer in the collection path with rotatable axis.

Theoretical Model: The CI method based on single-band EMA was used to treat the correlation energy beyond second order in perturbative expansion. To reduce the computational cost, only the blocks involving double excitations that directly connected to the multiexciton ground states were considered in the CI matrix. The single-particle basis states were obtained analytically from eigenvalues and eigenvectors of the noninteracting Hamiltonian in the EMA with the underlying impenetrable wall assumption. The N-particle basis was constructed as the tensor product of N single-particle bases. The effect of the dielectric confinement due to the presence of an external medium outside was approximated by using the multiplicative factor that was derived from second-order energy, which contained Coulomb interaction, in the spherical perturbative calculations. More details can be found in Section SII, Supporting Information.

Supporting Information

Supporting Information is available from the Wiley Online Library or from the author.

Acknowledgements

The authors acknowledge Dr. Frank Krumeich for having performed TEM characterization on the studied QDs. This project was funded by the European Union's Horizon 2020 program, through a FET Open research and innovation action under the grant agreement No. 899141 (PoLLoC). J.E. acknowledges financial support from the Institute Universitaire de France. C.Z, M.I.B., and G.R. acknowledge funding from the Swiss National Science Foundation (Grant No. 200021_192308, "Q-Light – Engineered Quantum Light Sources with Nanocrystal Assemblies"). The project was also partially supported by the Air Force Office of Scientific Research and the Office of Naval Research under award number FA8655-21-1-7013 and by the Swiss National Science Foundation (Grant No. 188404, "Novel inorganic light emitters: synthesis, spectroscopy and applications").

Conflict of Interest

The authors declare no conflict of interest.

Author Contributions

C.Z. and T.N. contributed equally to this work. The manuscript was written through contributions of all authors. All authors have given approval to the final version of the manuscript.

Data Availability Statement

The data that support the findings are openly available at the ETH Research Collection

Keywords

binding energies in exciton complexes, configuration interaction methods, $CsPbBr_3$ quantum dots, effective mass calculations, polarons, quantum correlations, single quantum dot spectroscopy

Received: September 12, 2022
Revised: November 25, 2022
Published online: January 18, 2023

[1] L. Protesescu, S. Yakunin, M. I. Bodnarchuk, F. Krieg, R. Caputo, C. H. Hendon, R. X. Yang, A. Walsh, M. V. Kovalenko, *Nano Lett.* **2015**, *15*, 3692.
[2] Q. A. Akkerman, G. Rainò, M. V. Kovalenko, L. Manna, *Nat. Mater.* **2018**, *17*, 394.
[3] Q. A. Akkerman, T. P. Nguyen, S. C. Boehme, F. Montanarella, D. N. Dirin, P. Wechsler, F. Beiglböck, G. Rainò, R. Erni, C. Katan, *Science* **2022**, *377*, 1406.
[4] F. Krieg, S. T. Ochsenbein, S. Yakunin, S. T. Brinck, P. Aellen, A. Süess, B. Clerc, D. Guggisberg, O. Nazarenko, Y. Shynkarenko, *ACS Energy Lett.* **2018**, *3*, 641.
[5] F. Zhang, H. Zhong, C. Chen, X.-g. Wu, X. Hu, H. Huang, J. Han, B. Zou, Y. Dong, *ACS Nano* **2015**, *9*, 4533.
[6] M. I. Bodnarchuk, S. C. Boehme, S. T. Brinck, C. Bernasconi, Y. Shynkarenko, F. Krieg, R. Widmer, B. Aeschlimann, D. Günther, M. V. Kovalenko, *ACS Energy Lett.* **2018**, *4*, 63.
[7] M. V. Kovalenko, L. Protesescu, M. I. Bodnarchuk, *Science* **2017**, *358*, 745.
[8] J. Song, J. Li, X. Li, L. Xu, Y. Dong, H. Zeng, *Adv. Mater.* **2015**, *27*, 7162.
[9] T. Chiba, K. Hoshi, Y.-J. Pu, Y. Takeda, Y. Hayashi, S. Ohisa, S. Kawata, J. Kido, *ACS Appl. Mater. Interfaces* **2017**, *9*, 18054.

[10] X. Lin, X. Dai, C. Pu, Y. Deng, Y. Niu, L. Tong, W. Fang, Y. Jin, X. Peng, *Nat. Commun.* **2017**, *8*, 1132.
[11] S. W. Eaton, M. Lai, N. A. Gibson, A. B. Wong, L. Dou, J. Ma, L.-W. Wang, S. R. Leone, P. Yang, *Proc. Natl. Acad. Sci. USA* **2016**, *113*, 1993.
[12] J. Pan, S. P. Sarmah, B. Murali, I. Dursun, W. Peng, M. R. Parida, J. Liu, L. Sinatra, N. Alyami, C. Zhao, *J. Phys. Chem. Lett.* **2015**, *6*, 5027.
[13] Y. Wang, X. Li, J. Song, L. Xiao, H. Zeng, H. Sun, *Adv. Mater.* **2015**, *27*, 7101.
[14] S. Yakunin, L. Protesescu, F. Krieg, M. I. Bodnarchuk, G. Nedelcu, M. Humer, G. De Luca, M. Fiebig, W. Heiss, M. V. Kovalenko, *Nat. Commun.* **2015**, *6*, 8515.
[15] F. Yan, S. T. Tan, X. Li, H. V. Demir, *Small* **2019**, *15*, 1902079.
[16] B. R. Sutherland, E. H. Sargent, *Nat. Photonics* **2016**, *10*, 295.
[17] Y. Fang, Q. Dong, Y. Shao, Y. Yuan, J. Huang, *Nat. Photonics* **2015**, *9*, 679.
[18] J. Gao, S. C. Nguyen, N. D. Bronstein, A. P. Alivisatos, *ACS Photonics* **2016**, *3*, 1217.
[19] P. Ramasamy, D.-H. Lim, B. Kim, S.-H. Lee, M.-S. Lee, J.-S. Lee, *ChemComm* **2016**, *52*, 2067.
[20] M. I. Saidaminov, M. A. Haque, M. Savoie, A. L. Abdelhady, N. Cho, I. Dursun, U. Buttner, E. Alarousu, T. Wu, O. M. Bakr, *Adv. Mater.* **2016**, *28*, 8144.
[21] B.-W. Hsu, Y.-T. Chuang, C.-Y. Cheng, C.-Y. Chen, Y.-J. Chen, A. Brumberg, L. Yang, Y.-S. Huang, R. D. Schaller, L.-J. Chen, *ACS Nano* **2021**, *15*, 11358.
[22] F. Hu, H. Zhang, C. Sun, C. Yin, B. Lv, C. Zhang, W. W. Yu, X. Wang, Y. Zhang, M. Xiao, *ACS Nano* **2015**, *9*, 12410.
[23] Y.-S. Park, S. Guo, N. S. Makarov, V. I. Klimov, *ACS Nano* **2015**, *9*, 10386.
[24] N. Yarita, H. Tahara, T. Ihara, T. Kawawaki, R. Sato, M. Saruyama, T. Teranishi, Y. Kanemitsu, *J. Phys. Chem. Lett.* **2017**, *8*, 1413.
[25] S. Pierini, M. d'Amato, M. Goyal, Q. Glorieux, E. Giacobino, E. Lhuillier, C. Couteau, A. Bramati, *ACS Photonics* **2020**, *7*, 2265.
[26] F. Hu, C. Yin, H. Zhang, C. Sun, W. W. Yu, C. Zhang, X. Wang, Y. Zhang, M. Xiao, *Nano Lett.* **2016**, *16*, 6425.
[27] B. Li, H. Huang, G. Zhang, C. Yang, W. Guo, R. Chen, C. Qin, Y. Gao, V. P. Biju, A. L. Rogach, *J. Phys. Chem. Lett.* **2018**, *9*, 6934.
[28] G. Rainò, G. Nedelcu, L. Protesescu, M. I. Bodnarchuk, M. V. Kovalenko, R. F. Mahrt, T. Stöferle, *ACS Nano* **2016**, *10*, 2485.
[29] H. Utzat, W. Sun, A. E. Kaplan, F. Krieg, M. Ginterseder, B. Spokoyny, N. D. Klein, K. E. Shulenberger, C. F. Perkinson, M. V. Kovalenko, *Science* **2019**, *363*, 1068.
[30] G. Rainò, M. A. Becker, M. I. Bodnarchuk, R. F. Mahrt, M. V. Kovalenko, T. Stöferle, *Nature* **2018**, *563*, 671.
[31] M. A. Becker, R. Vaxenburg, G. Nedelcu, P. C. Sercel, A. Shabaev, M. J. Mehl, J. G. Michopoulos, S. G. Lambrakos, N. Bernstein, J. L. Lyons, *Nature* **2018**, *553*, 189.
[32] M. A. Becker, L. Scarpelli, G. Nedelcu, G. Rainò, F. Masia, P. Borri, T. Stöferle, M. V. Kovalenko, W. Langbein, R. F. Mahrt, *Nano Lett.* **2018**, *18*, 7546.
[33] Y. Lv, C. Yin, C. Zhang, W. W. Yu, X. Wang, Y. Zhang, M. Xiao, *Nano Lett.* **2019**, *19*, 4442.
[34] R. Su, A. Fieramosca, Q. Zhang, H. S. Nguyen, E. Deleporte, Z. Chen, D. Sanvitto, T. C. Liew, Q. Xiong, *Nat. Mater.* **2021**, *20*, 1315.
[35] A. V. Zasedatelev, A. V. Baranikov, D. Sannikov, D. Urbonas, F. Scafirimuto, V. Y. Shishkov, E. S. Andrianov, Y. E. Lozovik, U. Scherf, T. Stöferle, *Nature* **2021**, *597*, 493.
[36] G. Yuan, C. Ritchie, M. Ritter, S. Murphy, D. E. Gómez, P. Mulvaney, *J. Phys. Chem.* **2017**, *122*, 13407.
[37] M. Fu, P. Tamarat, H. Huang, J. Even, A. L. Rogach, B. Lounis, *Nano Lett.* **2017**, *17*, 2895.
[38] C. Yin, L. Chen, N. Song, Y. Lv, F. Hu, C. Sun, W. Y. William, C. Zhang, X. Wang, Y. Zhang, *Phys. Rev. Lett.* **2017**, *119*, 026401.
[39] C. Yin, Y. Lv, X. Zhang, Y. Zhang, W. W. Yu, C. Zhang, Z.-G. Yu, X. Wang, M. Xiao, *J. Phys. Chem. Lett.* **2020**, *11*, 5750.
[40] L. Hou, P. Tamarat, B. Lounis, *Nanomaterials* **2021**, *11*, 1058.
[41] P. Tamarat, L. Hou, J.-B. Trebbia, A. Swarnkar, L. Biadala, Y. Louyer, M. I. Bodnarchuk, M. V. Kovalenko, J. Even, B. Lounis, *Nat. Commun.* **2020**, *11*, 6001.
[42] M. A. Becker, C. Bernasconi, M. I. Bodnarchuk, G. Rainò, M. V. Kovalenko, D. J. Norris, R. F. Mahrt, T. Stöferle, *ACS Nano* **2020**, *14*, 14939.
[43] K. Cho, T. Yamada, H. Tahara, T. Tadano, H. Suzuura, M. Saruyama, R. Sato, T. Teranishi, Y. Kanemitsu, *Nano Lett.* **2021**, *21*, 7206.
[44] Y. Louyer, L. Biadala, P. Tamarat, B. Lounis, *Appl. Phys. Lett.* **2010**, *96*, 203111.
[45] M. J. Fernée, B. N. Littleton, H. Rubinsztein-Dunlop, *ACS Nano* **2009**, *3*, 3762.
[46] M. Califano, A. Franceschetti, A. Zunger, *Phys. Rev. B* **2007**, *75*, 115401.
[47] F. V. Antolinez, F. T. Rabouw, A. A. Rossinelli, R. C. Keitel, A. Cocina, M. A. Becker, D. J. Norris, *Nano Lett.* **2020**, *20*, 5814.
[48] M. J. Fernée, C. Sinito, Y. Louyer, C. Potzner, T.-L. Nguyen, P. Mulvaney, P. Tamarat, B. Lounis, *Nat. Commun.* **2012**, *3*, 1287.
[49] B. Patton, W. Langbein, U. Woggon, *Phys. Rev. B* **2003**, *68*, 125316.
[50] J. Tischler, A. Bracker, D. Gammon, D. Park, *Phys. Rev. B* **2002**, *66*, 081310.
[51] F. B. Basset, S. Bietti, M. Reindl, L. Esposito, A. Fedorov, D. Huber, A. Rastelli, E. Bonera, R. Trotta, S. Sanguinetti, *Nano Lett.* **2018**, *18*, 505.
[52] V. Solovyev, I. Kukushkin, *Phys. Rev. B* **2009**, *79*, 233306.
[53] M. Ware, E. Stinaff, D. Gammon, M. Doty, A. Bracker, D. Gershoni, V. Korenev, Ş. Bădescu, Y. Lyanda-Geller, T. Reinecke, *Phys. Rev. Lett.* **2005**, *95*, 177403.
[54] S. Rodt, A. Schliwa, K. Pötschke, F. Guffarth, D. Bimberg, *Phys. Rev. B* **2005**, *71*, 155325.
[55] G. Lubin, G. Yaniv, M. Kazes, A. C. Ulku, I. M. Antolovic, S. Burri, C. Bruschini, E. Charbon, V. J. Yallapragada, D. Oron, *ACS Nano* **2021**, *15*, 19581.
[56] D. Oron, M. Kazes, U. Banin, *Phys. Rev. B* **2007**, *75*, 035330.
[57] R. Osovsky, D. Cheskis, V. Kloper, A. Sashchiuk, M. Kroner, E. Lifshitz, *Phys. Rev. Lett.* **2009**, *102*, 197401.
[58] J. Dana, T. Binyamin, L. Etgar, S. Ruhman, *ACS Nano* **2021**, *15*, 9039.
[59] J. Aneesh, A. Swarnkar, V. K. Ravi, R. Sharma, A. Nag, K. Adarsh, *J. Phys. Chem.* **2017**, *121*, 4734.
[60] M. N. Ashner, K. E. Shulenberger, F. Krieg, E. R. Powers, M. V. Kovalenko, M. G. Bawendi, W. A. Tisdale, *ACS Energy Lett.* **2019**, *4*, 2639.
[61] X. Shen, S. Wang, C. Geng, L. Li, E. Zhao, J. Sun, W. Wu, L. An, K. Pan, *J. Phys. Chem.* **2021**, *125*, 5278.
[62] J. A. Castaneda, G. Nagamine, E. Yassitepe, L. G. Bonato, O. Voznyy, S. Hoogland, A. F. Nogueira, E. H. Sargent, C. H. B. Cruz, L. A. Padilha, *ACS Nano* **2016**, *10*, 8603.
[63] K. E. Shulenberger, M. N. Ashner, S. K. Ha, F. Krieg, M. V. Kovalenko, W. A. Tisdale, M. G. Bawendi, *J. Phys. Chem. Lett.* **2019**, *10*, 5680.
[64] X. Huang, L. Chen, C. Zhang, Z. Qin, B. Yu, X. Wang, M. Xiao, *J. Phys. Chem. Lett.* **2020**, *11*, 10173.
[65] A. Mondal, J. Aneesh, V. K. Ravi, R. Sharma, W. J. Mir, M. C. Beard, A. Nag, K. Adarsh, *Phys. Rev. B* **2018**, *98*, 115418.
[66] C. Wolf, H. Cho, Y. H. Kim, T. W. Lee, *ChemSusChem* **2017**, *10*, 3705.
[67] A. K. Poonia, M. Shrivastava, W. J. Mir, J. Aneesh, A. Nag, K. Adarsh, *Phys. Rev. B* **2021**, *104*, L161407.
[68] V. I. Klimov, *Annu. Rev. Condens. Matter Phys.* **2014**, *5*, 285.
[69] C. Melnychuk, P. Guyot-Sionnest, *Chem. Rev.* **2021**, *121*, 2325.
[70] S. Bera, R. K. Behera, N. Pradhan, *J. Am. Chem. Soc.* **2020**, *142*, 20865.

[71] T. P. T. Nguyen, S. A. Blundell, C. Guet, *Phys. Rev. B* **2020**, *101*, 125424.
[72] G. Rainò, A. Landuyt, F. Krieg, C. Bernasconi, S. T. Ochsenbein, D. N. Dirin, M. I. Bodnarchuk, M. V. Kovalenko, *Nano Lett.* **2019**, *19*, 3648.
[73] S. N. Raja, Y. Bekenstein, M. A. Koc, S. Fischer, D. Zhang, L. Lin, R. O. Ritchie, P. Yang, A. P. Alivisatos, *ACS Appl. Mater. Interfaces* **2016**, *8*, 35523.
[74] I. Hwang, I. Jeong, J. Lee, M. J. Ko, K. Yong, *ACS Appl. Mater. Interfaces* **2015**, *7*, 17330.
[75] H. Huang, B. Chen, Z. Wang, T. F. Hung, A. S. Susha, H. Zhong, A. L. Rogach, *Chem. Sci.* **2016**, *7*, 5699.
[76] H. Huang, M. I. Bodnarchuk, S. V. Kershaw, M. V. Kovalenko, A. L. Rogach, *ACS Energy Lett.* **2017**, *2*, 2071.
[77] H. Zhang, X. Wang, Q. Liao, Z. Xu, H. Li, L. Zheng, H. Fu, *Adv. Funct. Mater.* **2017**, *27*, 1604382.
[78] R. Phillips, D. Lovering, G. Denton, G. Smith, *Phys. Rev. B* **1992**, *45*, 4308.
[79] E. P. Booker, M. B. Price, P. J. Budden, H. Abolins, Y. del Valle-Inclan Redondo, L. Eyre, I. Nasrallah, R. T. Phillips, R. H. Friend, F. Deschler, *Adv. Opt. Mater.* **2018**, *6*, 1800616.
[80] Y. You, X.-X. Zhang, T. C. Berkelbach, M. S. Hybertsen, D. R. Reichman, T. F. Heinz, *Nat. Phys.* **2015**, *11*, 477.
[81] D. Huber, M. Reindl, J. Aberl, A. Rastelli, R. Trotta, *J Opt* **2018**, *20*, 073002.
[82] N. Akopian, N. Lindner, E. Poem, Y. Berlatzky, J. Avron, D. Gershoni, B. Gerardot, P. Petroff, *Phys. Rev. Lett.* **2006**, *96*, 130501.
[83] A. Muller, W. Fang, J. Lawall, G. S. Solomon, *Phys. Rev. Lett.* **2009**, *103*, 217402.
[84] Y. Chen, J. Zhang, M. Zopf, K. Jung, Y. Zhang, R. Keil, F. Ding, O. G. Schmidt, *Nat. Commun.* **2016**, *7*, 10387.
[85] M. Bayer, A. Kuther, A. Forchel, A. Gorbunov, V. Timofeev, F. Schäfer, J. Reithmaier, T. Reinecke, S. Walck, *Phys. Rev. Lett.* **1999**, *82*, 1748.
[86] M. Isarov, L. Z. Tan, M. I. Bodnarchuk, M. V. Kovalenko, A. M. Rappe, E. Lifshitz, *Nano Lett.* **2017**, *17*, 5020.
[87] J. Ramade, L. M. Andriambariarijaona, V. Steinmetz, N. Goubet, L. Legrand, T. Barisien, F. Bernardot, C. Testelin, E. Lhuillier, A. Bramati, *Nanoscale* **2018**, *10*, 6393.
[88] J. Ramade, L. M. Andriambariarijaona, V. Steinmetz, N. Goubet, L. Legrand, T. Barisien, F. Bernardot, C. Testelin, E. Lhuillier, A. Bramati, *Appl. Phys. Lett.* **2018**, *112*, 072104.
[89] D. F. Macias-Pinilla, J. Planelles, J. I. Climente, *Nanoscale* **2022**, *14*, 8493.
[90] Y. Cho, S. M. Greene, T. C. Berkelbach, *Phys. Rev. Lett.* **2021**, *126*, 216402.
[91] O. Cannelli, N. Colonna, M. Puppin, T. C. Rossi, D. Kinschel, L. M. Leroy, J. Löffler, J. M. Budarz, A. M. March, G. Doumy, *J. Am. Chem. Soc.* **2021**, *143*, 9048.
[92] E. Cinquanta, D. Meggiolaro, S. G. Motti, M. Gandini, M. J. Alcocer, Q. A. Akkerman, C. Vozzi, L. Manna, F. De Angelis, A. Petrozza, *Phys. Rev. Lett.* **2019**, *122*, 166601.
[93] M. Puppin, S. Polishchuk, N. Colonna, A. Crepaldi, D. Dirin, O. Nazarenko, R. De Gennaro, G. Gatti, S. Roth, T. Barillot, *Phys. Rev. Lett.* **2020**, *124*, 206402.
[94] A. R. S. Kandada, C. Silva, *J. Phys. Chem. Lett.* **2020**, *11*, 3173.
[95] C. D. Sonnichsen, D. P. Strandell, P. J. Brosseau, P. Kambhampati, *Phys. Rev. Res.* **2021**, *3*, 023147.